Magnetic phase transition in two-phase multiferroics predicted from first principles

M. Fechner,[1] I. V. Maznichenko,[2] S. Ostanin,[1] A. Ernst,[1,3,*] J. Henk,[1] P. Bruno,[4] and I. Mertig[1,2]
[1]*Max-Planck-Institut für Mikrostrukturphysik, Weinberg 2, D-06120 Halle, Germany*
[2]*Institut für Physik, Martin-Luther-Universität Halle-Wittenberg, D-06099 Halle, Germany*
[3]*Donostia International Physics Center (DIPC), Paseo de Manuel Lardizabal 4, 20018 San Sebastin/Donostia, Basque Country, Spain*
[4]*European Synchrotron Radiation Facility, Boîte Postale 220, F-38043 Grenoble Cedex, France*
(Received 15 August 2008; published 11 December 2008)

On the basis of first-principles electronic-structure calculations we predict that epitaxial multiferroic films—fabricated as ultrathin Fe films deposited on TiO_2-terminated (001) surfaces of $ATiO_3$ perovskites (A =Pb,Ba)—exhibit an unexpected change in their magnetic structure with increasing Fe-film thickness. The magnetic order changes from ferromagnetic, with a magnetization of about $3\mu_B$/atom for the 1 ML system, to ferrimagnetic with almost vanishing magnetization upon deposition of a second Fe layer. Ferromagnetic order is restored for thicker Fe films but with significantly reduced magnetization as compared to Fe bulk. The effect is understood in terms of hybridization of electronic states and geometric structure. The magnetoelectric coupling affects the size of the magnetic moments moderately; a spin-reorientation transition is not found.

DOI: 10.1103/PhysRevB.78.212406 PACS number(s): 75.80.+q, 73.20.−r, 75.70.Ak, 77.84.−s

Epitaxial growth techniques open paths to assemble two-phase multiferroic films from ferroelectrics and ferromagnets (FMs). Inaccessible by conventional synthesis, they exhibit specific properties which are superior to those of customary materials.[1] Especially switching and spin filtering make them excellent candidates for next-generation magnetoelectronic devices, such as magnetic-field sensors and memories. Current efforts focus on the realization of prototypical devices which consist of a few-nanometer thick ferroelectric sandwiched between a ferromagnet and a metallic contact.[2,3]

The key feature of multiferroic devices is the magnetoelectric coupling. In a simple picture, the coupling between the electric polarization $\boldsymbol{P}$ (a result of atomic displacements) in the ferroelectric component and the magnetization $\boldsymbol{M}$ in the FM component is mediated by the hybridization of spin-polarized electronic states at the common interface. If the coupling is sufficiently strong, $\boldsymbol{M}$ can be modified by an external electric field. Analogously, $\boldsymbol{P}$ can be changed by an external magnetic field. This mechanism allows to store information in nanometer-sized memories[4,5] with four logic states, $(\pm\boldsymbol{P},\pm\boldsymbol{M})$. The quest for fundamentally different multiferroics requires evidently thorough understanding of the mechanisms which mediate the magnetoelectric coupling.

Prototypical two-phase multiferroic systems are heterojunctions of Fe and polar $ATiO_3$ perovskites, e.g., $BaTiO_3$ (BTO) and $PbTiO_3$ (PTO). The stable TiO_2-terminated (001) surface of the latter forms an electric dipole.[6] With the surface oxygen atoms displaced outward with respect to the Ti atoms for both $\boldsymbol{P}$ orientations, the intrinsic ferroelectricity is notably suppressed at the surface.[7] Hence, a critical thickness (typically 1 nm) is required to maintain ferroelectricity at room temperature.[8] Please note that little is known about the magnetic properties of $Fe/ATiO_3$ heterojunctions, in particular about the Fe-thickness dependence.[9,10]

Considering ultrathin Fe films on an $ATiO_3$ perovskite we are confronted with a delicate interplay between geometry, electronic properties, and magnetic structure. Since Fe has a tendency toward antiferromagnetism if the volume is reduced,[11] we expect a complex magnetic structure in $Fe/ATiO_3$ in dependence on the Fe-film thickness. Questions to be answered concern the magnetic order, the size of the magnetization, and the magnetic anisotropy. Further, one can ask for differences if a ferroelectric substrate (BTO, PTO) is replaced by a paraelectric, e.g., $SrTiO_3$ (STO). To predict the properties of these multiferroics reliably, sophisticated first-principles methods of computational materials science are inevitable.

In this Brief Report we report on a first-principles investigation of the magnetic order and the magnetoelectric effect in $(Fe_2)_L/ATiO_3(001)$ multiferroics with Fe-film thickness $L=1,\ldots,4$ monolayers (ML) on top of the TiO_2-terminated (001) surfaces of BTO, PTO, and STO. This choice of perovskite substrates allowed to model a variety of nanostructures, ranging from paraelectric to highly polar interfaces, with different in-plane misfits. The (001) surface was chosen TiO-terminated, according to its superior stability.[6] As striking result we find an unexpected change in the magnetic order from ferromagnetic ($L=1$) to ferrimagnetic order upon adding a second Fe layer ($L=2$). A sizable change in the magnetic structure appears due to reversal of $\boldsymbol{P}$, making these multiferroics very appealing for device applications.

The delicate interplay of geometric, electronic, and magnetic structures necessitates a multicode approach, which already proved successful.[12] The geometric relaxations were obtained by VASP,[13] well known for its precise determination of energetics and forces. The atomic positions serve as input for multiple-scattering calculations of the electronic and magnetic structure [scalar-relativistic Korringa-Kohn-Rostoker (KKR)].[14] The magnetocrystalline anisotropy was computed with a relativistic layer-KKR code.[15] In all steps, we applied the local spin-density approximation (LSDA) to density-functional theory. Various quantities were carefully cross-checked among the three computer codes to obtain consistent results. Reliability is achieved by numerous convergence tests.

The AO and TiO_2 planes in $ATiO_3$ perovskites (A =Ba,Pb,Sr) alternate in the [001] direction. In BTO and PTO, the atoms in each layer are mutually displaced along [001] (z axis); hence $\boldsymbol{P}$ is along that axis. For O atoms dis-

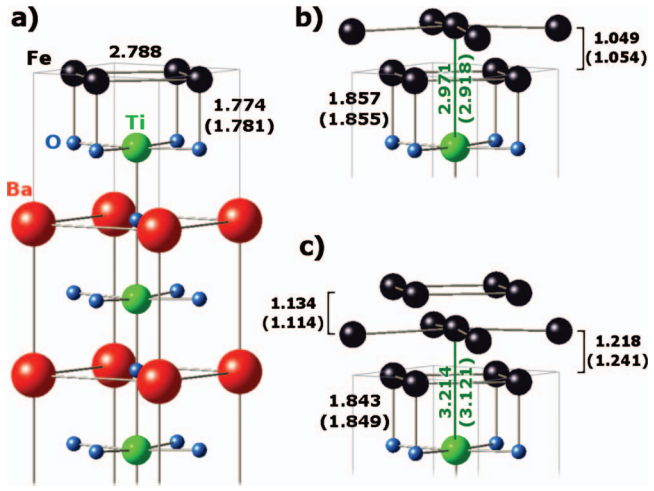

FIG. 1. (Color) Geometry of $(Fe_2)_L/BaTiO_3(001)$ for [left; (a)] $L=1$ and [right; (b) and (c)] $L=2,3$. Selected interatomic distances are given in angstroms for the $P_\downarrow(P_\uparrow)$ configuration without (within) brackets. Spheres represent Fe (black), Ba (red), Ti (green), and O (blue) sites. For $L=1$ (a), layers $\mathbf{S}+1,\ldots,\mathbf{S}-4$ are shown, while for $L=2$ (b) and $L=3$ (c) $\mathbf{S}+2,\ldots,\mathbf{S}$ and $\mathbf{S}+3,\ldots,\mathbf{S}$ are displayed, respectively.

placed along [001] with respect to the cations (Ba, Pb, and Ti), $\boldsymbol{P}$ points toward $[00\bar{1}]$, denoted $P_\downarrow$ here. For $P_\uparrow$, one has $\boldsymbol{P}$ pointing along [001] and opposite relaxations (for details, see Ref. 6). The intralayer buckling is defined for each layer l by $\delta_l = z_O - z_{cation}$. δ is positive (negative) for $P_\downarrow$ ($P_\uparrow$). For paraelectric STO, the displacements δ_l are zero.

The outermost TiO_2 layer in $Fe/ATiO_3$ is denoted $\mathbf{S}$. Layers toward the perovskite bulk are labeled $\mathbf{S}-1$, $\mathbf{S}-2$, etc., whereas Fe layers are indicated as $\mathbf{S}+1$, $\mathbf{S}+2,\ldots$, $\mathbf{S}+L$. As expected for $(Fe_2)_L/ATiO_3$, Fe forms a distorted body-centered tetragonal lattice, with the sites in layer $\mathbf{S}+1$ on top of the O sites in layer $\mathbf{S}$ (Fig. 1). In the following we focus on Fe on BTO.

The atomic positions deduced by VASP serve as input for the first-principles KKR calculations of the electronic and magnetic properties. Considering $L=1$, the Fe magnetic moments ($\approx 3\mu_B$) are significantly enhanced with respect to the Fe bulk value of $2.26\mu_B$ (Table I). The hybridization between the Fe $3d$, Ti $3d$, and O $2p$ states at the interface [layers $\mathbf{S}$ and $\mathbf{S}+1$; cf. the associated spin-resolved density of states in

TABLE I. Local magnetic moments of $(Fe_2)_L/BaTiO_3(001)$, $L=1,2,3$, for $P_\uparrow$ and $P_\downarrow$ obtained by KKR (in μ_B).

		$L=1$		$L=2$		$L=3$	
		$P_\uparrow$	$P_\downarrow$	$P_\uparrow$	$P_\downarrow$	$P_\uparrow$	$P_\downarrow$
Fe	$\mathbf{S}+3$					1.80	1.94
Fe	$\mathbf{S}+2$; Ti			−2.49	−2.40	1.91	1.93
Fe	$\mathbf{S}+2$; Ba			2.28	2.18	1.04	0.95
Fe	$\mathbf{S}+1$	3.02	3.05	0.22	0.26	1.05	0.94
O	$\mathbf{S}$	0.10	0.10	0	0	0.01	0.01
Ti	$\mathbf{S}$	−0.10	−0.04	−0.03	−0.02	−0.12	−0.05

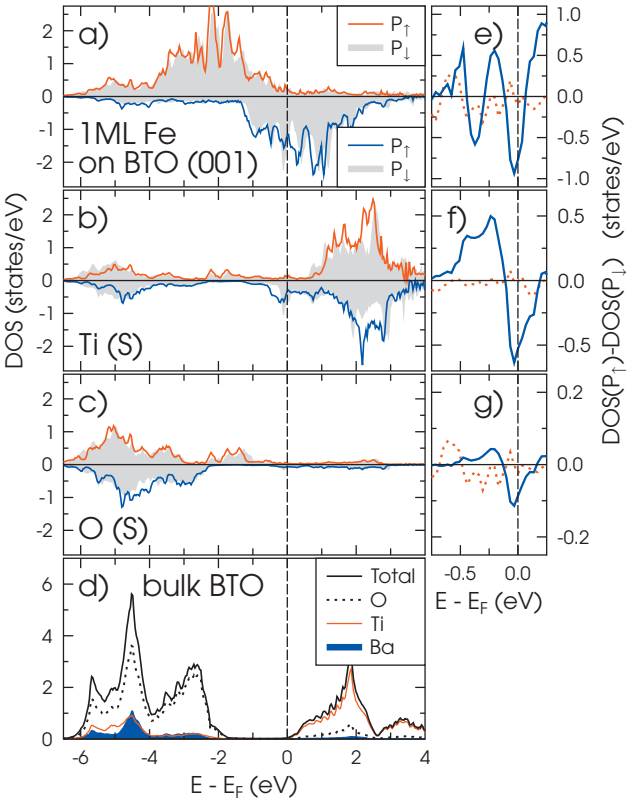

FIG. 2. (Color) Electronic structure at the surface of $(Fe_2)_1/BaTiO_3(001)$. [(a)–(c)]: spin-resolved density of states (DOS) of Fe in layer $\mathbf{S}+1$ (a) as well as of Ti (b) and O (c) in layer $\mathbf{S}$ for $P_\uparrow$ (lines) and $P_\downarrow$ (gray). (d) Total and partial DOS of bulk $BaTiO_3$, with the bottom of the conduction band taken as energy reference. [(e)–(g)] Spin-resolved difference of the DOS for $P_\uparrow$ and $P_\downarrow$ of Fe, Ti, and O [as in (a)–(c)] close to the Fermi energy E_F (majority: red dotted; minority: blue solid).

Figs. 2(a)–2(c)] induces magnetic moments in the interfacial O and Ti atoms. In particular the Ti moments, aligned antiparallel to those of Fe and O, originate from the hybridization of Ti $3d$ with minority-spin Fe $3d$ states.[9,10] Reversal of $\boldsymbol{P}$ affects the magnetic moments mildly (less than $0.06\mu_B$).

Adding a second Fe layer changes the magnetic order considerably (Table I, $L=2$): the magnetic moments in the Fe layer $\mathbf{S}+1$ are almost quenched while the sizable moments in the surface layer $\mathbf{S}+2$ are ordered antiparallel. Please note that the two Fe sites in $\mathbf{S}+2$ are inequivalent [Fig. 1(b)]; Fe($\mathbf{S}+2$;Ti) [Fe($\mathbf{S}+2$;Ba)] is on top of Ti (Ba) sites in layer $\mathbf{S}$. The different magnetic moments reflect the environment of these atoms, in particular the atomic volumes and the hybridization. Polarization reversal affects mainly the positions of Ti atoms and consequently those of the Fe atoms atop. For example, the z position of Fe($\mathbf{S}+2$;Ti) is changed by 0.053 Å, while that of Fe($\mathbf{S}+2$;Ba) is with about 0.005 Å less influenced [Fig. 1(b)]. The surface-layer buckling is 0.02 Å (0.04 Å) for $P_\downarrow(P_\uparrow)$.

Deposition of a third Fe layer restores the ferromagnetic order (Table I, $L=3$). The distance between Fe layers at the surface is about 1.1 Å, i.e., less than in bcc Fe(001) (1.43 Å). Reversal of the polarization attracts the upper two Fe layers with respect to Ti($\mathbf{S}$) about 0.03 Å, which is larger

than for $L=2$. Again, the position of the atom Fe($\mathbf{S}+2$;Ti) is subject to polarization switching: its z position is changed by 3% or 0.1 Å. Layers $\mathbf{S}+3$ and $\mathbf{S}+2$ contribute most to the total magnetization with a remarkable "magnetic imbalance" of the two inequivalent Fe sites in layer $\mathbf{S}+2$. Layer $\mathbf{S}+1$ contributes about $1\mu_B$. The largest change upon polarization switching shows up in the surface layer $\mathbf{S}+3$ ($0.14\mu_B$).

As is obvious from the preceding, the positions and the magnetic moments of the Fe atoms in the entire Fe films are determined in a complex manner by the Fe/BTO interface. We obtain two counteracting trends. First, the reduced coordination number at the Fe surface layer causes an increase in the magnetic moments. Second, the reduced atomic volume due to epitaxial strain of the BTO substrate and a drastic tetragonal distortion in comparison with Fe bulk, following Pauling's rule,[16] quench the magnetic moments.

For layer $\mathbf{S}+1$, the Fe-O distances which range from 1.78 to 1.85 Å for $L=1-3$ are substantially smaller than the interatomic distance in bulk bcc Fe. Hence, the diminished volume of interfacial Fe can lead to reduced local magnetic moments.[11] The magnetic moments for $L=1$ are still considerable due to the reduced dimensionality at the surface. For $L=2$, the volume of interfacial Fe is reduced even further and leads to the very small magnetic moments. The small size of Fe atoms in layer $\mathbf{S}+2$ explains as well the antiferromagnetic (AFM) ordering of their local magnetic moments.[11] Adding the third Fe layer increases both the coordination numbers and the atomic volumes and consequently restores ferromagnetic order.

While the magnetic moments do not change sign upon $\boldsymbol{P}$ reversal (only their sizes are moderately affected; Table I), we consider a spin-reorientation transition as another—possible—kind of magnetoelectric switching. Using relativistic layer KKR, the magnetic anisotropy for $(Fe_2)_1/BTO(001)$ is computed within the framework of the magnetic force theorem.[17] For both $\boldsymbol{P}$ orientations, perpendicular anisotropy is favored to in-plane anisotropy, namely, by 0.72 meV ($P_\downarrow$) and 0.54 meV ($P_\uparrow$) per Fe atom. Note that these uniaxial anisotropies are almost twice as large as that of a chemically disordered FePt alloy.[18,19]

The magnetoelectric coupling in $(Fe_2)_1/BTO(001)$ is further illustrated by the density of states at the interface [Figs. 2(e)–2(g)]. A prominent effect is evident in the minority-spin channel of the Fe- and Ti-electronic states while there is no significant effect in the majority channel. Thus, reversal of $\boldsymbol{P}$ leads to a substantial transfer of minority-spin charge at the interface.[20] Because the Fe-Ti distance for $P_\downarrow$ is smaller than for $P_\uparrow$, the overlap between the Fe and Ti d orbitals is larger, leading to an increased charge density in the surface layer $\mathbf{S}+1$ (Fig. 3). The excessive electrons result in a slightly larger magnetic moment of Fe for $P_\downarrow$ (Table I).

To address the effects of polarizability and lattice misfit on the magnetic structure of the Fe films, additional calculations were performed for Fe-covered PTO and STO. For all perovskite substrates and Fe-film thicknesses, total energies of three magnetic configurations were computed: besides FM and paramagnetic (PM) Fe films, AFM films were considered. In the latter case, the magnetic moments of the two Fe sites in each layer are oppositely oriented. The peculiarity of the case of $L=2$ becomes apparent by the fact that the con-

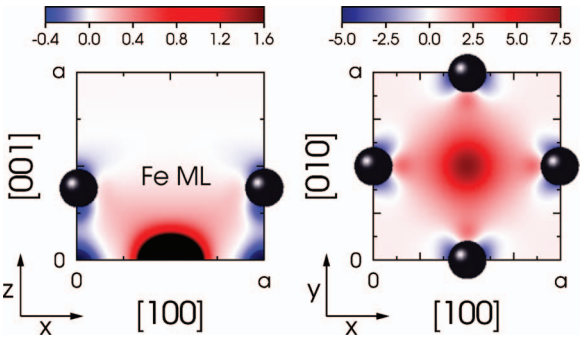

FIG. 3. (Color) Charge redistribution of minority-spin electrons at the surface of $(Fe_2)_1/BTO(001)$ upon reversal of the electric polarization $\boldsymbol{P}$ with respect to the surface normal. The difference of the charge densities for $P_\uparrow$ and $P_\downarrow$ is depicted in a perpendicular (left) and an in-plane cut through the Fe atoms (size a^2; color scales in arbitrary units). The Fe atoms are represented by spheres.

strained self-consistent calculations did not converge for the complete AFM configuration; forcing the top layer $\mathbf{S}+2$ to be antiferromagnetic, the layer $\mathbf{S}+1$ shows ferromagnetic order.

In almost all cases, the hierarchy $E_{FM}<E_{PM}<E_{AFM}$ is observed. An exception is again $L=2$ for which a ferrimagnetic order with small (absolute) magnetic moments is favored (Fig. 4; cf. Table I for Fe/BTO). Even in the case of paraelectric STO, both the magnetization and the total-energy hierarchy are similar to those of the polar substrates. Thus, the magnetic order of the two-phase multiferroics can be tuned by the Fe-film thickness independently of the perovskite substrate. Strain and electric polarizabilities are of minor importance. For each of the systems with $L=1$, the magnetoelectric coefficient α is estimated. α is defined as $\mu_B\Delta M/(VE_c)$ in terms of the magnetization change ΔM per volume V and strength of the coercive electric field E_c of the substrate. For the surface bilayer of Fe/BTO, $\mu_B\Delta M/V$

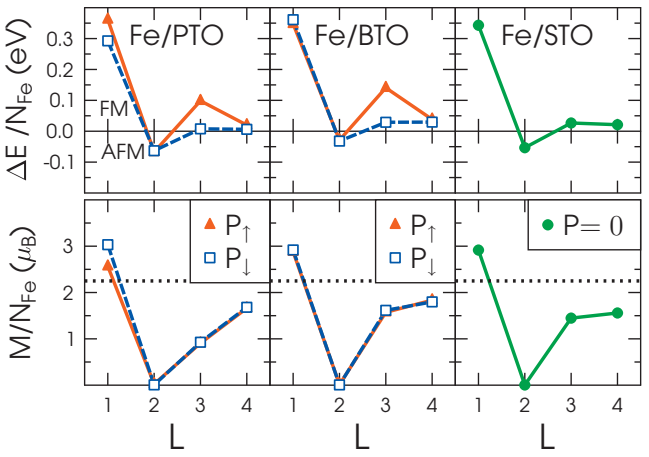

FIG. 4. (Color) Magnetism of $(Fe_2)_L/ATiO_3(001)$ for $PbTiO_3$, $BaTiO_3$, and $SrTiO_3$ versus Fe-film thickness L. Top: total-energy difference $\Delta E \equiv E_{AFM}-E_{FM}$ of the antiferromagnetic and ferromagnetic configurations (see text) normalized with respect to the number N_{Fe} of Fe atoms in the film unit cell. Bottom: magnetization per Fe atom for the lowest-energy configuration. Dotted lines indicate the magnetic moment of Fe bulk.

$\approx 1.6\times 10^2$ G and, assuming $E_c=10$ kV/cm, $\alpha\approx 0.016$ G cm/V, which is comparable with α measured in epitaxial $BiFeO_3/CoFe_2O_4$ nanostructures.[21] For Fe/PTO with $E_c=33$ kV/cm, $\mu_B\Delta M/V\approx 2.4\times 10^3$ G yields $\alpha\approx 0.073$ G cm/V, which is significantly larger than that of Fe/BTO.

In conclusion, the magnetic structure of two-phase multiferroics, realized as ultrathin Fe films on $ATiO_3$ perovskites (A=Ba,Pb,Sr), is found to exhibit a rich and peculiar structure, as is predicted from first-principles computational materials science. A ferromagnetic-to-ferrimagnetic transition which is accompanied by a strong reduction in the Fe magnetic moments could be used in device applications to tailor the properties of the magnetic subsystem. This effect mainly originated from the magnetovolume instability of Fe. In our opinion, a similar effect may occur as well in other materials, which exhibit the magnetovolume instability such as manganese[22] and gadolinium.[23] Significant magnetoelectric coupling via the Fe/$ATiO_3$ interface is predicted; a spin-reorientation transition under switching is not found. In view of device applications it appears highly desirable to investigate theoretically and experimentally the thickness-dependent magnetic properties of Fe films sandwiched between ferroelectric perovskites.

We acknowledge useful conversations with H. Meyerheim. This work was supported by the DFG *Forschergruppe* 404 "Oxidic Interfaces" and by the *Sonderforschungsbereich* SFB 762, "Functionality of Oxidic Interfaces." M.F. is a member of the International Max Planck Research School for Science and Technology of Nanostructures.

*aernst@mpi-halle.de

[1] M. Dawber, K. M. Rabe, and J. F. Scott, Rev. Mod. Phys. **77**, 1083 (2005).
[2] N. Hur, S. Park, P. A. Sharma, J. S. Ahn, S. Guha, and S.-W. Cheong, Nature (London) **429**, 392 (2004).
[3] M. Gajek, M. Bibes, S. Fusil, K. Bouzehouane, J. Fontcuberta, A. Barthélémy, and A. Fert, Nature Mater. **6**, 296 (2007).
[4] W. Eerenstein, N. D. Mathur, and J. F. Scott, Nature (London) **442**, 759 (2006).
[5] S.-W. Cheong and M. Mostovoy, Nature Mater. **6**, 13 (2007).
[6] M. Fechner, S. Ostanin, and I. Mertig, Phys. Rev. B **77**, 094112 (2008).
[7] J. Junquera and P. Ghosez, Nature (London) **422**, 506 (2003).
[8] D. D. Fong, G. B. Stephenson, S. K. Streiffer, J. A. Eastman, O. Auciello, P. H. Fuoss, and C. Thompson, Science **304**, 1650 (2004).
[9] C.-G. Duan, S. S. Jaswal, and E. Y. Tsymbal, Phys. Rev. Lett. **97**, 047201 (2006).
[10] J. P. Velev, C.-G. Duan, K. D. Balashchenko, S. S. Jaswal, and E. Y. Tsymbal, J. Appl. Phys. **103**, 07A701 (2008).
[11] T. C. Leung, C. T. Chan, and B. N. Harmon, Phys. Rev. B **44**, 2923 (1991).
[12] C. R. Ast, J. Henk, A. Ernst, L. Moreschini, M. C. Falub, D. Pacilé, P. Bruno, K. Kern, and M. Grioni, Phys. Rev. Lett. **98**, 186807 (2007).
[13] G. Kresse and J. Furthmüller, Phys. Rev. B **54**, 11169 (1996).
[14] M. Lüders, A. Ernst, W. M. Temmerman, Z. Szotek, and P. J. Durham, J. Phys.: Condens. Matter **13**, 8587 (2001).
[15] J. Henk, H. Mirhosseini, P. Bose, K. Saha, N. Fomynikh, T. Scheunemann, S. V. Halilov, E. Tamura, and R. Feder, OMNI—Fully relativistic electron spectroscopy calculations, 2008; the computer code is available from the authors.
[16] L. Pauling, *The Nature of the Chemical Bond* (Cornell University Press, Ithaca, 1960).
[17] J. Henk, A. M. N. Niklasson, and B. Johansson, Phys. Rev. B **59**, 9332 (1999).
[18] S. Ostanin, S. S. A. Razee, J. B. Staunton, B. Ginatempo, and E. Bruno, J. Appl. Phys. **93**, 453 (2003).
[19] J. B. Staunton, S. Ostanin, S. S. A. Razee, B. L. Gyorffy, L. Szunyogh, B. Giatempo, and Ezio Bruno, Phys. Rev. Lett. **93**, 257204 (2004).
[20] R. D. King-Smith and D. Vanderbilt, Phys. Rev. B **47**, 1651(R) (1993).
[21] F. Zavaliche, H. Zheng, L. Mohaddes-Ardabili, S. Y. Yang, Q. Zhan, P. Shafer, E. Reilly, R. Chopdekar, Y. Jia, P. Wright *et al.*, Nano Lett. **5**, 1793 (2005).
[22] V. L. Moruzzi, P. M. Marcus, and J. Kübler, Phys. Rev. B **39**, 6957 (1989).
[23] I. D. Hughes, M. Däne, A. Ernst, W. Hergert, M. Lüders, J. Poulter, J. B. Staunton, A. Svane, Z. Szotek, and W. M. Temmerman, Nature (London) **446**, 650 (2007).